COMPTON SCATTER AND X-RAY CROSSTALK AND THE USE OF VERY THIN INTER-CRYSTAL SEPTA IN HIGH RESOLUTION PET DETECTORS

C.S. Levin, M.P. Tornai, S.R. Cherry, L.R. MacDonald, E.J. Hoffman
Div. of Nuclear Medicine & Biophysics and Imaging Sciences Division, Crump Institute for Biological Imaging, UCLA School of Medicine

Abstract

To improve spatial resolution, PET systems are being developed with finer detector elements. Unfortunately, using smaller crystal sizes increases inter-crystal Compton scatter and bismuth x-ray and (to a lesser degree) electron escape crosstalk, causing positioning errors that lead to degradation of image contrast. We investigated the use of extremely thin (≤ 300 μm) lead strips for passive shielding of this inter-crystal crosstalk. Using annihilation photons and small (2 and 3 mm wide) BGO crystals in coincidence, crosstalk studies were performed with either two small adjacent crystals (1-D) or one crystal inside a volume of BGO (2-D). The fraction of Compton scattered events from one crystal into an adjacent one was reduced, on average, by a factor of 3.2 (2.2) in the 1-D experiment and by a factor of 3.0 (2.1) in 2-D, with a 300 (150) μm thick lead strip in between the crystals and a 300-700 keV energy window in both crystals. We could not measure a reduction in bismuth x-ray crosstalk with the use of lead septa because of the production of lead x-rays. The width of the coincident point spread function was not significantly different for the 1- and 2-D studies, with or without the different thickness septa in place. These results indicate that intercrystal crosstalk does not affect the positioning resolution. A simple insertion of very thin lead strips may significantly reduce the inter-crystal scattering crosstalk of a high resolution PET system, thereby ultimately improving image contrast, without introducing a dead area.

I. INTRODUCTION

Current advances in PET detector technology have resulted in and are moving toward the development of systems with smaller detector elements designed to further improve spatial resolution. Unfortunately utilizing smaller crystal sizes leads to a higher fraction of inter-crystal crosstalk due to Compton scattering. It has been suggested that inter-crystal scattering is the primary cause of event mispositioning in high resolution block detectors used in commercial PET systems [1]. Similar crosstalk effects occur in high resolution discrete-crystal designs.

For ≤ 3 mm wide crystals, we have observed that bismuth K-shell x-ray and electron escape cross talk also play a significant role. These low energy effects result from the incomplete energy deposition of a gamma ray interaction in a crystal. The 1/e length of an 80 keV bismuth x-ray in BGO is approximately 0.2 mm. The average range of a 511 keV photoelectron in BGO is roughly 0.1 mm. Because 511 keV gamma ray interactions result in both Compton- and photo-electron production, most electrons created will have energies much less than 511 keV. In addition, because an electron deposits its energy continuously in the crystal, the remaining energy after it escapes the crystal will be low, on average. Thus, the electron escape contribution of the low energy crosstalk will be small in comparison to that due to the 80 keV bismuth escape x-ray.

The conventional method used to reduce the effects of Compton scattering is energy thresholding on the photopeak. However, this method is somewhat limited when the energy resolution is poor (as is the case for systems using BGO as the scintillator) and ultimately reduces the system sensitivity. We investigated the use of extremely thin lead strips (≤ 0.3 mm) for passive shielding of inter-crystal crosstalk using measurements with a ^{22}Na source of 511 keV annihilation photons and small, square BGO crystals (2 and 3 mm width) in coincidence. In previous work [2-4], intercrystal septa was for the most part introduced in the context of improving the spatial resolution uniformity across the imaging area (camera field of view) in conjunction with wedge shaped or tapered crystals. In those investigations, larger crystals (≥ 4 mm) and septa (≥ 1 mm) widths were utilized. The implementation of these relatively thick septa necessarily reduced the total geometrical efficiency (ring sensitivity) by reducing the crystal packing fraction. It was concluded that the benefits did not outweigh the disadvantages.

We are interested in studying the effect of introducing very fine intercrystal septa (≤0.3 mm) between small (2-3 mm) crystals. This fine septa can be, for example, inserted in between crystals in current PET detector designs [1] without reducing the packing fraction (introducing a dead area): These designs already have 250-400μm intercrystal spaces for reflector and the amount of reflector can be reduced with little loss in light output.

In our measurements we will use different energy thresholds to take into account the possible contribution of intercrystal crosstalk of different energies.

II. MATERIALS AND METHODS

A. One-Dimensional Experiment

Experiments were performed using two different thicknesses of lead inter-crystal septa, 0.15 and 0.30 mm, placed in between two crystals, for both 2x2x10 and 3x3x30 mm^3 crystal sizes. Figure 1 shows a top-down schematic drawing of the one-dimensional experimental set-up. Two crystals of the same size were coupled sideways (for better light collection efficiency) with optical grease to two separate 1.5" diameter RCA PMTs. Three layers of thin teflon tape covered the non-detecting faces of each crystal and black tape surrounded the crystal borders on each tube. The two PMTs + the crystals (D1 and D2) were then pressed together face on so that the sides of the crystals were in line with each other with or without the thin lead septa in place. There was no measurable light leak between crystals. A third BGO crystal

0-7803-3180-X/96$5.00©1996

(2x2x30 mm^3) was coupled to another PMT end on and covered with teflon and black tape (D3). This third crystal was used as the electronic back-collimating detector and was placed approximately 20 cm away from the other two detectors so that the axis of the third crystal was in line with the axis of D1.

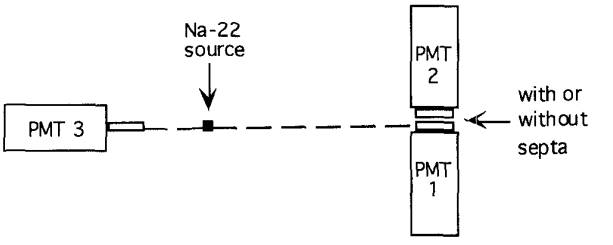

Fig. 1. Schematic of top view of set-up for the 1-D experiment. PMT 1 and 3 coupled to small crystals (referred to as D1 and D3, respectively) are in coincidence.

The electronic configuration was as follows: The outputs from all three detectors were first amplified. Signals from D1 and D2 were split into two parts: the first set went into Constant Fraction Discriminators (TENNELEC TC454, ≤ 10 ns gate for both channels) with a low threshold (just above the noise) and then into a coincidence unit (EG&G C315) followed by a gate and delay generator (EG&G 416A); The second set of signals was amplified and shaped (ORTEC 855, 1μs shaping time) and digitized (BiRa 907). The digitizers were triggered on a coincidence between D3 and D1 (see Fig. 1). Digitized detector values of D1 and D2 were collected in list mode on a Macintosh computer through a GPIB interface to CAMAC via LabView (National Instruments).

A ^{22}Na source (~2 μCi), positioned approximately 8 cm from D3, was moved perpendicular to the line between D3 and D1 in 0.5 mm steps and the CPSF was measured with or without the thin lead strips in place. Source size and positron range in the plastic source holder are roughly 1 and 0.8 mm, respectively. Events observed in D2 when D1 and D3 are set in coincidence are considered to be a result of inter-crystal crosstalk (Compton scatter, bismuth x-ray or electron escape). The energy spectra of D1 and D2 with various thresholds (lower and upper) applied were extracted from the post-processed list mode data. In list mode all energy depositions in D1 and D2 were accepted and various energy thresholds (upper and lower) were applied in post-processing.

We define *scatter fraction* as the ratio of the number of events recorded in D2 to those in D1 for a given common energy threshold in both detectors and source position. We note that this definition of scatter fraction might only be appropriate when the collimated source is directly positioned over D1 (the crystal of interest). Because we are interested in the CPSF we have loosely extended this definition to include those source positions where it is, by geometry, more likely that the gamma ray is interacting in D2 first before scattering into D1 (D1 must be hit for trigger). The *scatter fraction reduction factor* is defined as the ratio of scatter fraction without to that with inter-crystal septa in place between the two crystals. These definitions represent an average over the number of counts in the measured energy spectrum of D1 and D2 above a given threshold. For example, if a 300 keV threshold is chosen in both detectors, then for a given event at most one detector can have >300 keV deposited within (511 keV maximum) and count in our definition of scatter fraction. For lower energy thresholds, such as 150 keV, both detectors can contribute to the measure of scatter fraction.

We also measured the ratio R=(d1-d2)/(d1+d2) per event, where d1 and d2 represent the pulse heights measured from the respective detectors. This ratio, R, is analogous to that used for positioning in multiplexed crystal array designs and was measured for source positions collimated directly over D1.

B. *Two-Dimensional Experiment*

Figure 2 shows a schematic of the experimental set-up used to measure the effects of completely surrounding a 2 x 2 x 30 mm^3 crystal with lead septa and a volume of BGO. The general concept is the same as in the 1-D experiment except only D1 and D2 are shown in Figure 2. The back-collimating detector, D3, is approximately 13 cm away from D1, and the ^{22}Na source half-way between the two. As seen in Figure 2, the scintillation light from the large BGO crystals that comprise D2 (which surrounds D1) is read out from the top with a PMT. Again the source was moved perpendicular to the D1-D3 line in 0.5 mm steps and the CPSF and scatter fraction measured with and without lead septa surrounding D1.

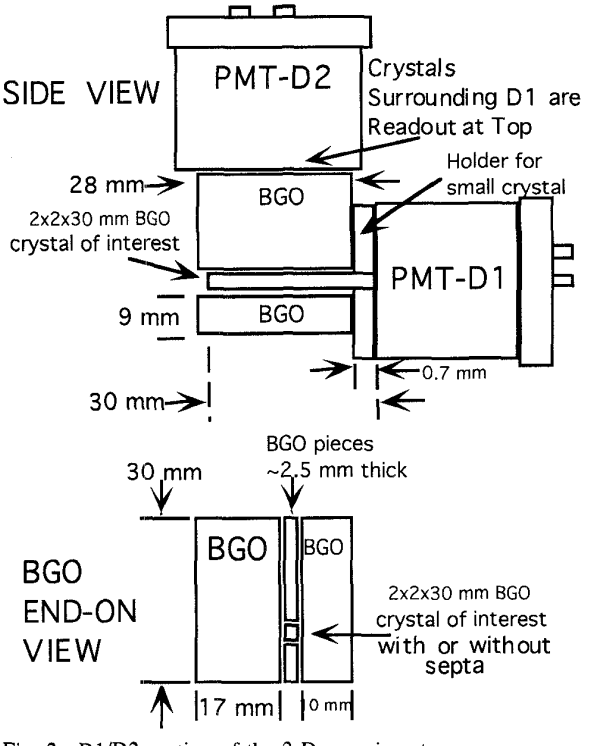

Fig. 2. D1/D2 portion of the 2-D experiment.

Two additional effects were studied with the 2-D experiment: the contribution to the inter-crystal cross-talk due to the 80 keV Bismuth K-shell x-ray, and, possibly, electron escape. We note however, that electron escape will effect crosstalk, at best, only within a 0.1 mm perimeter of a crystal (19% of the cross-sectional area of a 2 mm wide crystal), whereas, on average, an 80 keV bismuth x-ray will play a role within the outer 0.2 mm of the same crystal (36% of the cross-sectional area of a 2 mm wide BGO crystal). Thus, the 80 bismuth x-ray escape will play a dominant role in low energy crosstalk (see Section I). With a 150 keV threshold set on D1

the total number of counts in D2 for 57-97 and 30-125 keV energy windows were measured for 5 collimated source positions over D1. The electron escape events deposit a continuum of energies weighted toward lower energies. The second energy window will thus encompass a larger proportion of electron escape events. We will use the crosstalk fraction measured in this latter window to roughly access the combined contribution of escape x-ray and electron. For the smaller (57-97 keV) energy window, we will assume the counts are due only to bismuth x-ray crosstalk. The ratio of the number of events in observed in D2 within these energy windows to that in D1 is the fraction of events that will be mispositioned.

III. RESULTS

A. 1-D Experiment: Coincident Point Spread Function and Energy Spectra:

Figure 3 shows the CPSF measured in D1 and crosstalk into D2 for a 300 keV lower and 700 keV upper energy threshold in each of D1 and D2 ($2x2x10mm^3$) with and without a 0.3 mm lead strip in place for the 1-D experiment. The FWHM of the CPSF of D1 (1.54 mm) was measured to be only 3% narrower (only one side has the adjacent crystal) with the 0.3 mm septa in place. Note the different peak positions of the CPSF of D1 and D2. The maximum of the CPSF of D1 occurs where the source position is in line with the center of the crystal. Figure 4 shows the corresponding full energy spectra (no threshold) measured in the crystals with and without the 0.3 mm septa.

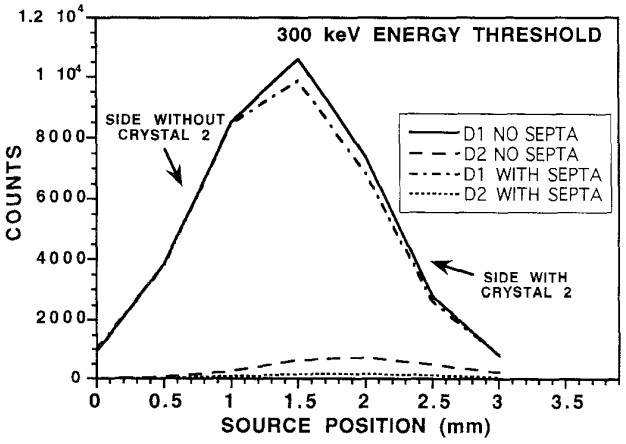

Fig. 3. Measured coincident point spread function (CPSF) of D1 for a 1 mm diameter ^{22}Na point source with and without a 0.3 mm thick lead strip in place between D1 and D2 (see Fig.1) for a 300 keV energy threshold.

B. 1-D Experiment: Scatter Fraction:

Figure 5 shows the scatter fraction measured in D2 for a 300 keV lower and 700 keV upper energy threshold in each of the 2 x 2 x 10 mm^3 crystals, with and without the 0.3 mm thick septa in place as a function of source position. We note that the definition of scatter fraction given in Section II might be most appropriate when the source position is collimated over D1, but this quantity is also shown for positions outside of D1 (position 1.5 is the center of D1).

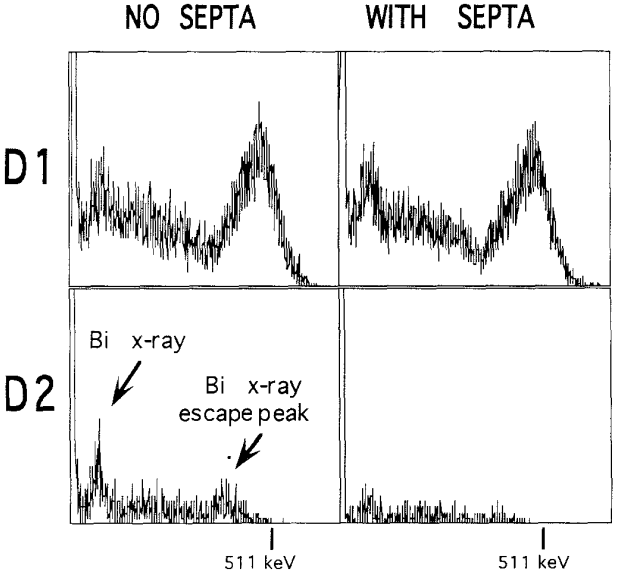

Fig. 4 The unthresholded energy spectra in both detectors when the source was electronically collimated on the center of D1. The vertical scale of the D2 spectra shown has been enlarged by a factor of two relative to that of D1.

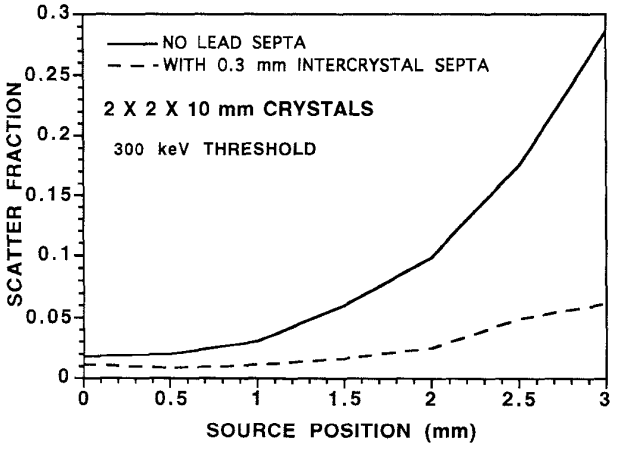

Fig. 5. Scatter fraction versus source position with and without the 0.3 mm lead septa in place (300 keV threshold in D1 and D2).

Figure 6 shows the scatter fraction reduction factor achieved with the 0.30 mm lead strip in place as a function of various source positions and energy thresholds. For a 300 keV energy threshold, we found that the fraction of scattered events into an adjacent crystal was reduced, on average, by a factor of 3.2 (2.1) when there was a 0.30 (0.15) mm thick lead strip in place. In general, this reduction factor depended on energy threshold (see energy spectra in Fig. 2) and source position. With the lead strips in place between larger 3 x 3 x 30 mm^3 crystals, we found similar results for the scatter fraction reduction factor: the larger crystals had, within 10%, approximately the same scatter fraction above a 300 keV energy threshold for points directly over the D1 crystal (but had a higher count rate).

In Figure 7 we show a different way of representing the scatter data. Let d1 and d2 be the digitized pulse heights per event of the signals from D1 and D2, respectively. Figure 7

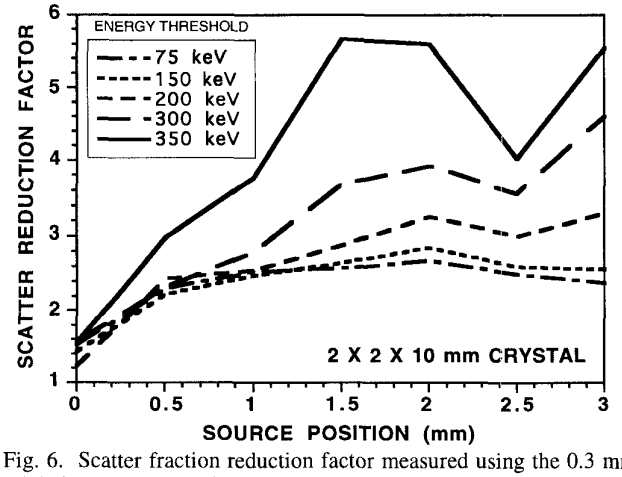

Fig. 6. Scatter fraction reduction factor measured using the 0.3 mm thick intercrystal lead septa as a function of source position for various energy thresholds (2 x 2 x 10 mm^3 BGO crystal). The dip seen is approximately at the position of the septa.

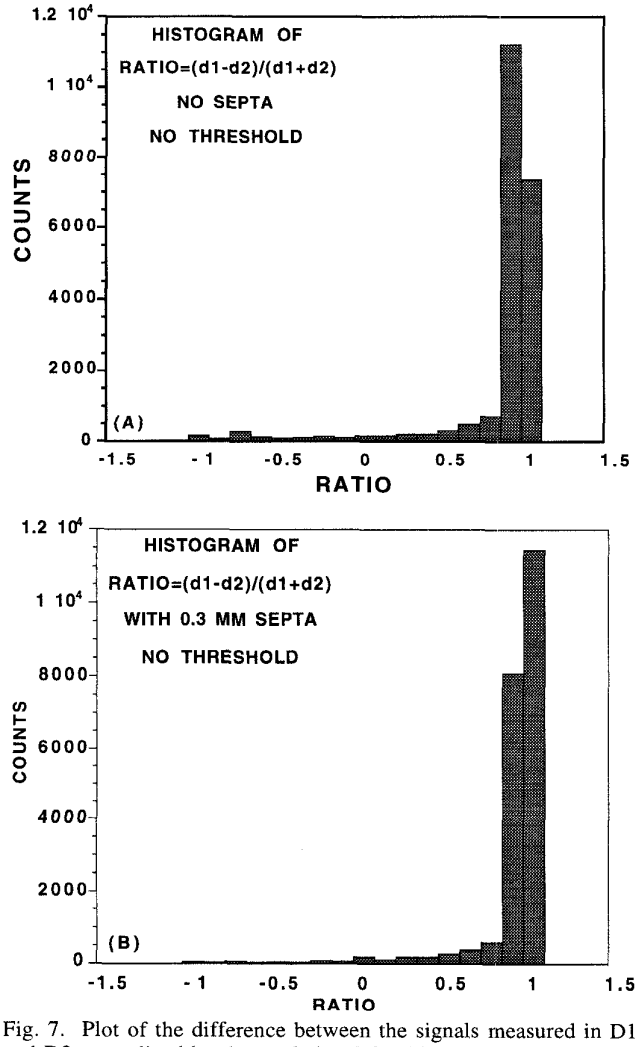

Fig. 7. Plot of the difference between the signals measured in D1 and D2 normalized by the total signal for (a) no septa and (b) with 0.3 mm septa for the 1-D experiment (Fig. 1). The presence of the septa reduces the errors in positioning (the correct position is a ratio of 1). All energies were used.

shows a histogram of ratio (d1-d2)/(d1+d2) per event with and without the 0.3 mm septa present. This ratio is the 1-D analogy of that used to position events in multiplexed (light sharing) PET block detector designs [1]. We see the deviation from the correct position (a ratio of 1) lessens with the septa in place. This representation is especially relevant to multiplexed crystal array designs where all of the light (or charge) created from all the crystals in the array per event is used for crystal identification (positioning) and energy thresholding of that event. From this figure one can better access the contribution of crosstalk to mispositioning errors in an array, without the presence of light sharing effects [1].

C. 2-D Experiment: Coincident Point Spread Function:

Figure 8 shows the CPSF measured in D1 and crosstalk component seen in D2 for a 300 keV lower and 700 keV upper energy threshold in both detectors with and without the two sizes of lead septa (0.15 and 0.30 mm) in place. There is no significant difference in the CPSF FWHM or FWTM between the 1- and 2-D experiments, even though there is a much greater BGO scatter volume present and nearly 4 times the scatter fraction. Furthermore, there is no change in these quantities with the introduction of septa. These results will be discussed in Section IV.

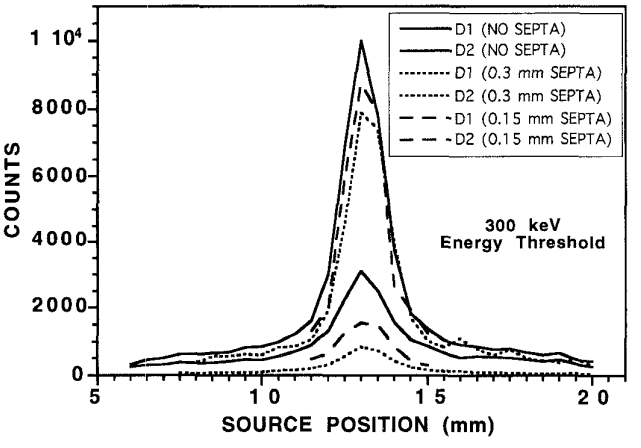

Fig. 8. Coincident PSF measured for D1 and crosstalk measured in D2 as a function of source position for no septa and with 0.15 mm and 0.3 mm thick lead septa completely surrounding D1 (300 keV lower and 700 keV upper energy thresholds in D1 and D2). Upper 3 curves: response of D1, Lower 3 curves: D2.

D. 2-D Experiment: Scatter Fraction

Figure 9 displays the fractional crosstalk (top) and crosstalk reduction (bottom) for 150 and 300 keV thresholds measured in D2 with no septa and with 0.15 and 0.3 mm septa in place. For source positions directly over D1, since the energy thresholds are high in this figure, the x-ray escape peak of bismuth is not contributing. The scatter fraction is improved, on average, by a factor of 3.0 (2.1) with the 0.3 (1.5) mm septa in place.

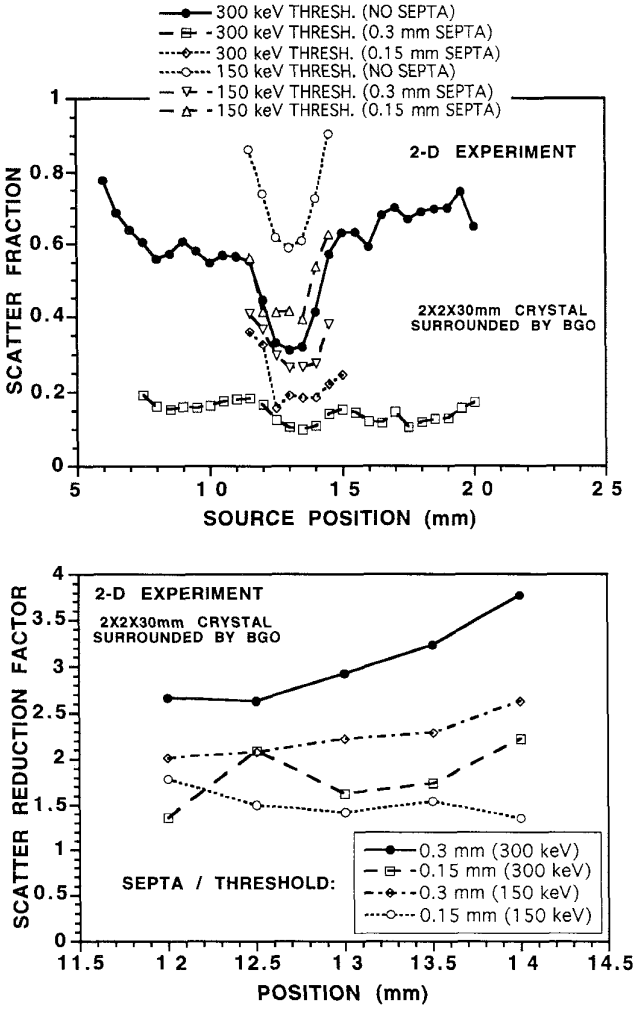

Fig. 9. Top: Scatter fraction vs. source position for no septa, 0.15 and 0.3 mm lead septa. The data shows measurements with thresholds of both 150 and 300 keV in D1 and D2. Bottom: Corresponding scatter reduction factor.

E. Cross-Talk Due to X-Ray and Electron Escape

Figure 10 displays the crosstalk from D1 into D2 for a lower energy window in D2 centered about the 77 keV bismuth x-ray with and without septa in place. Bismuth x-ray crosstalk into D2 (with no septa) is roughly 10% of events registered in D1 for a 50% energy window centered about 77 keV (57-97 keV) and a lower energy threshold of 150 keV set in D1. For a 95 keV window about 77 keV the estimation of the combined x-ray and electron escape crosstalk is 25%. We observed an increase in x-ray crosstalk when 0.15 and 0.30 mm septa is used. This is due to the fact that gamma rays interacting with lead also produce 80 keV lead x-rays. There will be thus competing effects of gamma and bismuth x-ray (and electron) attenuation in the lead (crosstalk reduction) and lead x-ray production.

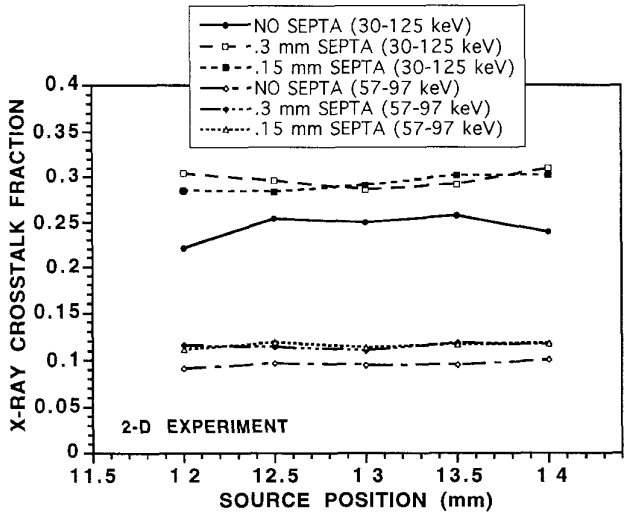

Fig. 10. X-ray and electron escape crosstalk into D2 from D1 vs. source position for 2-D experiment for two energy windows. In both cases a lower energy threshold of 150 keV was set in D1. The presence of lead septa slightly increases crosstalk at low energies due to lead 80 keV lead x-rays produced.

IV. DISCUSSION

In this experiment neither crosstalk (Compton scatter, bismuth x-ray and electron escape) nor intercrystal septa appeared to affect the intrinsic resolution as measured by the width of the coincident point spread function (CPSF). The CPSF width is a measure of the intrinsic resolution of an array. In this experiment, this quantity is determined by the crystal size, the size of the point source and the positron range in the source holder. The crosstalk sources do cause positioning errors which reduce image contrast. Our results indicate that with the simple insertion of very thin lead strips between ≤3 mm wide crystals, the crosstalk due to Compton scatter can be reduced significantly. Whether an improvement in image contrast would be worth the slight cost increase is open for debate.

V. REFERENCES

[1] SR Cherry, MP Tornai, CS Levin, S Siegel and EJ Hoffman. A Comparison of PET Detector Modules Employing Rectangular and Round Photomultiplier Tubes. *IEEE Trans. Nucl. Sci.* **42-4**, August 1995: 1064-8.

[2] NA Keller and LR Lupton. PET Detector Ring Aperture Function Calculations using Monte Carlo Techniques. *IEEE Trans. Nucl. Sci.* **NS-30-1**, February 1983, 676-80.

[3] JM Roney, CJ Thompson. Detector Identification with Four BGO Crystals on a Dual PMT. *IEEE Trans. Nucl. Sci.* NS-**31**: 1022-7, 1984.

[4] R Lecomte, D Schmitt and G Lamoureux. Geometry Study of a High Resolution PET Detection System Using Small Detectors. *IEEE Trans. Nucl. Sci.* **NS-31-1**, February 1984: 556-61.